Nuclear longitudinal form factors for axially deformed charge distributions expanded by nonorthogonal basis functions *

Jian Liu(刘健) [1;1)] Jinjuan Zhang(张进娟) [2] Chang Xu (许昌) [3] Zhongzhou Ren(任中洲) [3,4]

[1] College of Science, China University of Petroleum (East China), Qingdao 266580, China
[2] College of Electronic, Communication and Physics, Shandong University of Science and Technology, Qingdao 266590, China
[3] Department of Physics and Key Laboratory of Modern Acoustics, Nanjing University, Nanjing 210093, China
[4] Center of Theoretical Nuclear Physics, National Laboratory of Heavy-Ion Accelerator, Lanzhou 730000, China

Abstract: In this paper, the nuclear longitudinal form factors are systematically studied from the intrinsic charge multipoles. For axially deformed nuclei, two different types of density profiles are used to describe their charge distributions. For the same charge distributions expanded with different basis functions, the corresponding longitudinal form factors are derived and compared with each other. Results show the multipoles C_λ of longitudinal form factors are independent of the basis functions of charge distributions. Further numerical calculations of longitudinal form factors of ^{12}C indicates that the C_0 multipole reflects the contributions of spherical components of all nonorthogonal basis functions. For deformed nuclei, their charge RMS radii can also be determined accurately by the C_0 measurement. The studies in this paper examine the model-independent properties of electron scattering, which are useful for interpreting electron scattering experiments on exotic deformed nuclei.

Keywords: deformed charge distribution, elastic electron scattering, multipole matrix elements

PACS: 21.10.Ft, 25.30.Bf, 23.20.Js **DOI:** 10.1088/1674-1137/41/5/054101

1 Introduction

Electron scattering is an effective tool to probe the sizes and shapes of nuclei [1–6]. Interactions between electrons and nucleons are mainly via the electromagnetic force, which makes electrons relatively clean probes. Since the 1950s, the charge densities of many stable nuclei have been determined accurately by the electron scattering experiments [7, 8]. More recently, some new properties have been found in the exotic nuclei far away from the β stability line [9, 10], for example the neutron and proton halos, which are all related to the nucleon density distributions. Therefore, it is significant to explore the charge distributions of exotic nuclei with electron scattering. For this purpose, new experiments studying elastic electron scattering off exotic nuclei are now under way at RIKEN and GSI [11–15].

Meanwhile, much effort in the last decade has been devoted to theoretical studies [16–23]. Many methods have been developed to study electron scattering. The plane-wave Born approximation (PWBA) is a simple method which is widely used in calculating Coulomb multipoles C_λ [24–31] and magnetic multipoles M_λ [32–35] of form factors. The distorted-wave Born approximation (DWBA) method is more accurate than PWBA because the Coulomb distortion effect is considered [36, 37]. Many DWBA calculations have been performed studying the C_0 multipoles of exotic nuclei [19–23]. Furthermore, C_2 multipoles of inelastic electron scattering have also been investigated based on DWBA calculations in Refs. [38, 39].

The nuclear form factors are closely related to the intrinsic charge and current mutipoles [3, 40, 41]. The C_0 multipoles are attributed to the spherically symmetric ground state charge distribution and the C_2 multipole is proportional to the nuclear quadrupole moment Q. Most nuclei have deformation in their ground states [42–48]. The charge distributions of axially deformed nuclei can be described by the multiple expansion of spherical harmonics [49, 50]. Based on this expansion, the C_λ of longitudinal form factors can be investigated [3]. Besides the orthogonal bases, the deformed charge distributions can also be constructed with the nonorthogonal bases in some special case. In Ref. [30], the angular dependence

Received 22 November 2016, revised 26 January 2017

∗ Supported by National Natural Science Foundation of China (11505292, 11175085, 11575082, 11235001, 11275138, and 11447226), by Shandong Provincial Natural Science Foundation, China (BS2014SF007), Fundamental Research Funds for Central Universities (15CX02072A).

1) E-mail: liujian@upc.edu.cn

of charge distributions are described by the term $|Y_{20}(\theta,\varphi)|^2$. With this formalism, the author studied the parity-violating electron scattering off ^{27}Al [30]. By the comparative analysis in charge multipoles C_λ of Refs. [3, 30], one can see that for charge distributions described by different density profiles, charge multipoles C_λ always have different expressions. Therefore, in this paper we construct axially deformed charge distributions with different basis functions and analyze the corresponding longitudinal form factors. In this way the model-independent properties of electron scattering can be examined.

In this paper, we investigate the nuclear longitudinal form factors. For nuclei with axial deformation, the angular dependence of charge density distributions are expanded by the orthogonal bases and nonorthogonal bases, respectively. Then the C_0 and C_2 multipoles of longitudinal form factors are derived under the PWBA method for two different types of density profiles. By comparing the results, the validity of electron scattering is examined, and indicates that electron scattering is a model-independent way to study the nuclear charge distributions. With the derived formula, the longitudinal form factors of ^{12}C are investigated by both the PWBA and DWBA methods, where the corresponding charge distributions are described by the nonorthogonal bases. Numerical results show that by the C_0 measurements, spherical components of deformed charge distributions together with nuclear charge RMS radii can be accurately determined.

The paper is organized as follows. In Section 2 the longitudinal form factors of deformed nuclei are presented. In Section 3, the longitudinal form factors are calculated by both the PWBA and DWBA methods, and the results are compared with the experimental data. ^{12}C is chosen as the candidate. A summary is given in Section 4.

2 Theoretical framework

According to the contributions from Coulomb and magnetic interactions, the nuclear electromagnetic form factors $F(q)$ can be developed as the superposition of longitudinal terms $F_{\rm L}^2(q^2)$ and magnetic terms $F_{\rm M}^2(q^2)$. In the plane-wave Born approximation (PWBA), the longitudinal form factor is given by the Fourier transformation of the transition density $\rho_{\rm fi}(\boldsymbol{r})$ [41]:

$$|F_C(q)|^2 = \frac{1}{Z^2}\sum_{M_{\rm i}M_{\rm f}}|\rho(q)|^2, \tag{1}$$

where

$$\rho(q) = \int {\rm e}^{{\rm i}\boldsymbol{q}\cdot\boldsymbol{r}}\,\langle J_{\rm f}M_{\rm f}|\hat{\rho}(\boldsymbol{r})|J_{\rm i}M_{\rm i}\rangle\,{\rm d}^3r. \tag{2}$$

Multiply expanding the exponential function ${\rm e}^{i\boldsymbol{q}\cdot\boldsymbol{r}}$ and substituting it into Eq. (2), $\rho(q)$ can be rewritten as:

$$\begin{aligned}\rho(q) &= 4\pi\sum_{\lambda\mu} i^\lambda(-1)^\mu Y_{\lambda,\mu}(\hat{q})\\ &\quad\times\int {\rm d}^3r j_\lambda(qr)Y_{\lambda,-\mu}(\hat{r})\langle\alpha_{\rm f}|\hat{\rho}(\boldsymbol{r})|\alpha_{\rm i}\rangle\\ &= 4\pi\sum_{\lambda\mu} i^\lambda(-1)^\mu Y_{\lambda,\mu}(\hat{q})\\ &\quad\times\langle\alpha_{\rm f}|M(C\lambda,-\mu,q)|\alpha_{\rm i}\rangle,\end{aligned} \tag{3}$$

where $\langle\alpha_{\rm f}|M(C\lambda,\mu,q)|\alpha_{\rm i}\rangle$ is the scattering matrix. $|\alpha_{\rm i}\rangle$ and $|\alpha_{\rm f}\rangle$ represent the initial state $|J_{\rm i}M_{\rm i}\rangle$ and final state $|J_{\rm f}M_{\rm f}\rangle$. The Wigner-Eckart theorem can be used to factor out the dependence of $M(C\lambda,\mu,q)$ on the quantum numbers:

$$\begin{aligned}\langle\alpha_{\rm f}|M(C\lambda,\mu,q)|\alpha_{\rm i}\rangle &= (-1)^{J_{\rm i}-M_{\rm i}}\frac{1}{\sqrt{2\lambda+1}}\\ &\langle J_{\rm f}M_{\rm f},J_{\rm i}M_{\rm i}|J_{\rm f}J_{\rm i},\lambda\mu\rangle\langle J_{\rm f}||M(C\lambda,q)||J_{\rm i}\rangle.\end{aligned} \tag{4}$$

Substituting Eqs. (3) and (4) into Eq. (1), and taking into account the orthogonality of the Clebsch-Gordan (C. G.) coefficients, the longitudinal form factor can be given as [41, 51]:

$$\begin{aligned}|F_C(q)|^2 &= \frac{1}{Z^2}\frac{4\pi}{2J_{\rm i}+1}\sum_{\lambda=0,{\rm even}}^{\infty}|\langle\alpha_{\rm f}||M(C\lambda,q)||\alpha_{\rm i}\rangle|^2\\ &= |F_{C_0}(q)|^2+|F_{C_2}(q)|^2+|F_{C_4}(q)|^2+\cdots.\end{aligned} \tag{5}$$

From this formula, one can see that the longitudinal form factor can be decomposed into several multipoles by selection rules, such as C_0, C_2 and C_4 etc.

The specific form of $|F_{C_0}(q)|^2$ and $|F_{C_2}(q)|^2$ can be further extracted by the intrinsic multipoles. The Hamiltonian of the electric λ-pole transition can be written as [52]:

$$\begin{aligned}H^C_{\lambda,m} &= (4\pi/\omega q^2)\int\rho Y^*_{\lambda m}(\theta,\phi)\\ &\quad\times\left[\int Y_{\lambda m}(\theta',\phi')(\boldsymbol{q}\cdot\boldsymbol{j}_{\rm e}){\rm d}\Omega'\right]{\rm d}\tau,\end{aligned} \tag{6}$$

where $\boldsymbol{j}_{\rm e}=ec\boldsymbol{a}{\rm e}^{{\rm i}\boldsymbol{q}\cdot\boldsymbol{r}}$ is the transition current density arising from the change in the state of the electron. $\boldsymbol{a}$ is the matrix element of the Dirac $\boldsymbol{\alpha}$ operator between initial and final electron plane wave states of momenta, and c is the velocity of the electron. The integral of the solid angle Ω' makes the charge form factor independent of the momentum transfer $\mathbf{q}$. The integral in the square bracket vanishes unless $m=0$ and Eq. (6) turns into:

$$\begin{aligned}H^C_{\lambda,0} &= -(4\pi i^\lambda ea_0/q^2)[4\pi(2\lambda+1)]^{\frac{1}{2}}\\ &\quad\times\int\rho\cdot j_\lambda(qr)Y_{\lambda,0}\,{\rm d}\tau,\end{aligned} \tag{7}$$

where a_0 is the matrix element of the Dirac unit operator between initial and final electron states. By summation of Eq. (7), we can obtain:

$$\sum_{\lambda} H^{C}_{\lambda,0} = -(4\pi e a_0/q^2)\int \mathrm{e}^{\mathrm{i}\boldsymbol{q}\cdot\boldsymbol{r}}\rho\,\mathrm{d}\tau, \tag{8}$$

which is consistent with Eqs. (1) and (2).

From Eq. (7), the longitudinal form factor for multipoles $\lambda=0,2$ can be calculated as [52]:

$$|F_C|^2 = (2\lambda+1)^{-1}\cdot \sum_m \left|(4\pi)^{\frac{1}{2}}\int\left[j_0(qr)Y_{00} - f_m\sqrt{5}j_2(qr)Y_{20}\right]\rho\,\mathrm{d}\tau\right|^2. \tag{9}$$

$f_m=[3m^2-\lambda(\lambda+1)]/[\lambda(2\lambda-1)]$ is the relation between the intrinsic multipole and the transition multipole for $\lambda=2$. Because $\sum_m f_m=0$, the interference term between multipoles $\lambda=0$ and $\lambda=2$ vanishes and the longitudinal form factor can be given as:

$$\begin{aligned}|F_C(q)|^2 &= |F_{C_0}(q)|^2+|F_{C_2}(q)|^2\\ &= 4\pi\left[\int\rho_C(\boldsymbol{r})j_0(qr)Y_{00}\,\mathrm{d}\tau\right]^2\\ &\quad +14\pi\left[\int\rho_C(\boldsymbol{r})j_2(qr)Y_{20}\,\mathrm{d}\tau\right]^2,\end{aligned} \tag{10}$$

where $\rho_C(\boldsymbol{r})$ is the deformed charge density distribution. The C_2 multipole is proportional to the nuclear quadrupole moment Q. The observed quadrupole moment Q can be obtained from the intrinsic quadrupole moment Q_0:

$$Q=\frac{\lambda(2\lambda-1)}{(\lambda+1)(2\lambda+3)}\cdot Q_0, \tag{11}$$

where $\lambda=2$ and the intrinsic quadrupole moment Q_0 is:

$$Q_0=\left(\frac{16\pi}{5}\right)^{\frac{1}{2}}\int\rho_C Y_{20}\,\mathrm{d}\tau. \tag{12}$$

2.1 Charge distributions described by orthogonal bases

For nuclei with rotational symmetry, the multiple decomposition of the charge density distributions can be described by the multiple expansion of the spherical harmonics [49, 50]:

$$\rho_C(r,\theta)=\sum_{l=0}^{\text{even}}\rho_l(r)Y_{l0}(\theta,\varphi). \tag{13}$$

Combining this formula and Eq. (10), contributions of different multipoles l of deformed charge densities to the C_0 and C_2 of the longitudinal form factor can be investigated:

$$\begin{aligned}|F_C(q)|^2 &= |F_{C_0}(q)|^2+|F_{C_2}(q)|^2\\ &= 4\pi\left(\int_0^\infty r^2 j_0(qr)\rho_0(r)\mathrm{d}r\right)^2\\ &\quad +14\pi\left(\int_0^\infty r^2 j_2(qr)\rho_2(r)\mathrm{d}r\right)^2,\end{aligned} \tag{14}$$

which indicates that only the spherical part $\rho_0(r)$ contributes to the C_0 multipole and the quadrupoly deformed part $\rho_2(r)$ contributes to the C_2 multipole of longitudinal form factor. The multipoles ($l\geqslant 4$) of charge distributions in Eq. (13) have no effect on C_0 and C_2 due to the orthogonality of the spherical harmonics.

2.2 Charge distributions described by nonorthogonal bases

Instead of Eq. (13), the nuclear charge distributions can also be described by other density profiles. In Ref. [30], the author constructed the deformed part of density distributions with $|Y_{20}(\theta,\varphi)|^2$ and studied the C_2 multipoles for the odd-A nucleus ^{27}Al. If the angular dependence of nuclear charge density is described by $|Y_{20}(\theta,\varphi)|^2$, it can be written as:

$$\rho_C(r,\theta)=\rho_0'(r)+\rho_2'(r)\cdot|Y_{20}(\theta,\phi)|^2. \tag{15}$$

Substituting it into Eq. (10), we can obtain:

$$\begin{aligned}|F_C(q)|^2 &= |F_{C_0}(q)|^2+|F_{C_2}(q)|^2\\ &= \left[4\pi\int_0^\infty r^2 j_0(qr)\left(\rho_0'(r)+\frac{\rho_2'(r)}{4\pi}\right)\mathrm{d}r\right]^2\\ &\quad +\frac{10}{7}\left(\int_0^\infty r^2 j_2(qr)\rho_2'(r)\mathrm{d}r\right)^2.\end{aligned} \tag{16}$$

From Eq. (16), one can see there is an additional term $\frac{\rho_2'(r)}{4\pi}$ for the C_0 multipole, which is due to the contributions of the deformed part $|Y_{20}(\theta,\phi)|^2$ term in the nuclear charge densities. Equation (16) shows that for the specific model, the longitudinal multipoles have special formulas. If the charge distribution is constructed by the nonorthogonal bases, the deformed part may also contribute to the C_0 multipole. However, Eq. (16) does not conflict with the previous result Eq. (14), because the charge density distribution in Eq. (15) is not expressed based on the orthogonal basis. If the charge distribution of Eq. (15) is decomposed with the spherical harmonics of Eq. (13), we can obtain the relation:

$$\rho_0'(r) = \frac{\rho_0(r)}{2\sqrt{\pi}} + \frac{7\sqrt{5}}{20\sqrt{\pi}}\rho_2(r),$$
$$\rho_2'(r) = 7\sqrt{\frac{\pi}{5}}\rho_2(r). \tag{17}$$

Substituting this relation into Eq. (16), one can see that Eq. (16) is identical to Eq. (14).

Combining Eqs. (13)–(16), one can see that for the same charge distribution, the longitudinal form factors calculated with the orthogonal basis functions and nonorthogonal basis functions are identical with each other. For the deformed charge distributions described by the orthogonal basis functions, only the spherical part of charge distribution has an effect on the C_0 multipole. For deformed charge distributions described by the nonorthogonal basis functions, the C_0 multipole actually reflects the spherical components of all nonorthogonal basis functions.

3 Numerical results and discussion

In the previous section, we found that the C_0 multipole can constrain the spherical parts of the charge distribution, even described by the nonorthogonal basis functions. Based on the formula of Section 2, in this section charge form factors are numerically calculated where the charge distribution are constructed with the nonorthogonal basis functions. The nucleus ^{12}C is chosen as the candidate. In many previous studies on electron scattering, calculations were based on the spherical RMF model and DWBA method [16–23]. However, for ^{12}C, the spherical RMF model plus DWBA method cannot obtain reasonable charge form factors [53]. The discrepancy between the results of the spherical RMF model and experimental data indicates the differences in charge distribution between theory and experiment. Therefore, we add a deformation correction term to the spherical RMF charge density to describe the charge form factor of ^{12}C in this section.

First, the nuclear charge density is obtained by the spherical relativistic mean-field (RMF) model. In the RMF model, the effective Lagrangian density is [54, 55]:

$$\begin{aligned}\mathcal{L} = \bar{\psi}\Bigg[&\gamma^\mu\left(\mathrm{i}\partial\mu - g_\omega\omega_\mu - \frac{g_\rho}{2}\boldsymbol{\tau}\cdot\boldsymbol{\rho}_\mu - \frac{e}{2}(1+\tau^3)A_\mu\right)\\ &-(M-g_\mathrm{s}\sigma)\Bigg]\psi\\ &+\frac{1}{2}\partial^\mu\sigma\partial_\mu\sigma - \frac{1}{2}m_\sigma^2\sigma^2 - \frac{\kappa}{3!}(g_\mathrm{s}\sigma)^3 - \frac{\lambda}{4}(g_\mathrm{s}\sigma)^4\\ &-\frac{1}{4}\Omega^{\mu\nu}\Omega_{\mu\nu} + \frac{1}{2}m_\omega^2\omega^\mu\omega_\mu + \frac{\xi}{4!}(g_\omega^2\omega^\mu\omega_\mu)^2\\ &-\frac{1}{4}\boldsymbol{R}^{\mu\nu}\cdot\boldsymbol{R}_{\mu\nu} + \frac{1}{2}m_\rho^2\boldsymbol{\rho}^\mu\cdot\boldsymbol{\rho}_\mu\\ &-\frac{1}{4}F^{\mu\nu}F_{\mu\nu} + U_\mathrm{eff}(\omega_\mu,\boldsymbol{\rho}^\mu),\end{aligned} \tag{18}$$

where the self-interacting term of nonlinear ω-ρ coupling is taken as:

$$U_\mathrm{eff}(\omega_\mu,\boldsymbol{\rho}^\mu) = \Lambda_\mathrm{v}(g_\rho^2\boldsymbol{\rho}^\mu\vec{\rho}_\mu)(g_\omega^2\omega^\mu\omega_\mu). \tag{19}$$

Using the Euler-Lagrange equation, we can obtain the Dirac equations for nucleons and Klein-Gordon equations for mesons and photons. Based on the no-sea approximation and mean-field approximation, the motion equations can be solved iteratively, and the wave functions of the nucleons can be obtained. Then the nuclear proton density distribution can be obtained. Folding the proton charge distribution $\rho_\mathrm{p}(\boldsymbol{r})$ with the single proton charge distribution $\rho^\mathrm{p}(\boldsymbol{r})$, the RMF charge density can be calculated by the formula [56]:

$$\rho_\mathrm{R}(\boldsymbol{r}) = \int \rho_\mathrm{p}(\boldsymbol{r}')\rho^\mathrm{p}(\boldsymbol{r}-\boldsymbol{r}')\mathrm{d}r'. \tag{20}$$

The single proton charge distribution $\rho^\mathrm{p}(r)$ is:

$$\rho^\mathrm{p}(r) = \frac{Q^3}{8\pi}\mathrm{e}^{-Qr}, \tag{21}$$

where $Q = 0.71\,\mathrm{GeV}^2$.

Calculated by the spherical RMF model with the FSU parameter set, we obtain the spherical charge distribution $\rho_\mathrm{R}(r)$ of ^{12}C and investigate the its longitudinal form factor. However, for ^{12}C there are significant differences between the theoretical results and experimental data, which can be seen from Fig. 1. Therefore we assume the density profile of ^{12}C has a distribution like Eq. (15), which consists of two parts: a spherical part $\rho_0'(r)$ and a deformation correction $\rho_2'(r)\cdot|Y_{20}(\theta,\phi)|^2$. The spherical part $\rho_0'(r)$ is approximately described by the spherical RMF charge density $\rho_\mathrm{R}(r)$ with the FSU parameter set, and the deformed part $\rho_2'(r)$ is constructed by stretching $\rho_\mathrm{R}(r)$ with a factor χ. Finally, the charge density distribution is written as:

$$\begin{aligned}\rho_\mathrm{c}(r,\theta) &= \rho_0'(r) + \rho_2'(r)\cdot|Y_{20}(\theta,\phi)|^2\\ &= f\left(\rho_\mathrm{R}(r) + \frac{\xi}{\chi^3}\rho_\mathrm{R}(r/\chi)\cdot|Y_{20}(\theta,\phi)|^2\right),\end{aligned} \tag{22}$$

where ξ and χ are two tunable parameters, and f is the normalizing parameter of the charge number. Combining this formula with Eq. (16), the charge form factors of ^{12}C can be studied under the PWBA method. By adjusting the parameters ξ and χ in Eq. (22), the shape of the longitudinal form factor changes and the diffraction minimum shifts around. Fitting the experimental data, the tunable parameters are taken to be $\xi=-0.65$ and $\chi=0.58$, and the corresponding longitudinal form factors are presented in Fig. 1. For the purposes of comparison, the longitudinal form factor calculated by the spherical RMF charge density with the FSU parameter set is also presented in this figure. One can see that by taking into account the deformed part with Eq. (22) in the charge density distribution, the theoretical longitudinal form factor coincides with the experimental data much better for ^{12}C. Besides the longitudinal form factor, the nuclear intrinsic quadrupole moment is also calculated. Taking Eq. (22) into Eq. (12), the intrinsic quadrupole moment of ^{12}C is $Q_0=1.12$ fm^2, and this value is sensitive to the parameters ξ and χ in Eq. (22).

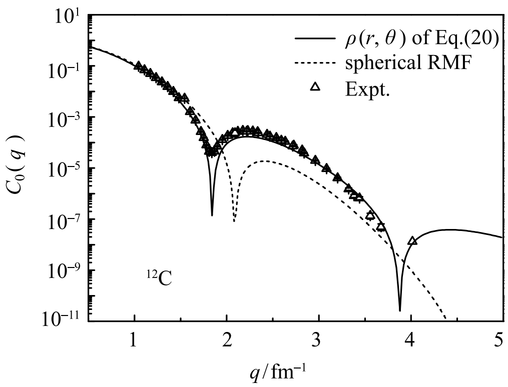

Fig. 1. Charge form factors of ^{12}C calculated by the PWBA method. The dotted line is obtained by the spherical RMF charge density $\rho_{\rm R}(r)$ with the FSU parameter set. The solid line is calculated by Eq. (16) where the corresponding charge density is described by Eq. (22). The experimental data are taken from Refs. [7, 57].

From Fig. 1 and Eq. (16), an equivalent spherical density distribution $\rho_{\rm Eq}(r)=\rho_0'(r)+\dfrac{1}{4\pi}\rho_2'(r)$ can be obtained for deformed charge densities described by Eq. (15) with nonorthogonal basis functions. $\rho_{\rm Eq}(r)$ represents the spherical components of all nonorthogonal basis functions. By comparing the theoretical longitudinal form factors with the experimental data, the equivalent spherical density $\rho_{\rm Eq}(r)$ of ^{12}C are extracted and presented in Fig. 2. The RMF charge density $\rho_{\rm R}(r)$ calculated by the FSU parameter set and experimental charge density $\rho_{\rm Ex}(r)$ described by the Fourier-Bessel (FB) model are also presented in this figure for comparison. There are differences between the RMF charge density $\rho_{\rm R}(r)$ and experimental charge density $\rho_{\rm Ex}(r)$ for ^{12}C. However, the equivalent spherical density $\rho_{\rm Eq}(r)$ is very close to the $\rho_{\rm Ex}(r)$. Figure 2 indicates that the spherical experimental charge density $\rho_{\rm Ex}(r)$ represents the equivalent spherical density $\rho_{\rm Eq}(r)$ of the deformed charge densities described with the nonorthogonal basis functions. For the charge density of Eq. (15), the RMS radius of the equivalent spherical charge density $\rho_{\rm Eq}(r)$ is also identical to the radii of the actual deformed charge density and the experimental spherical charge density:

$$\begin{aligned}\langle r^2\rangle &= \frac{1}{Z}\iint\left(\rho_0'(r)+\rho_2'(r)\cdot|Y_{20}(\theta,\phi)|^2\right){\rm d}r{\rm d}\Omega\\ &=\frac{4\pi}{Z}\int\left(\rho_0'(r)+\frac{\rho_2'(r)}{4\pi}\right)r^4\,{\rm d}r\\ &\simeq\frac{4\pi}{Z}\int\rho_{\rm Ex}(r)\,r^4\,{\rm d}r,\end{aligned}\tag{23}$$

which means that electron scattering is a model-independent method to measure the nuclear charge RMS radii.

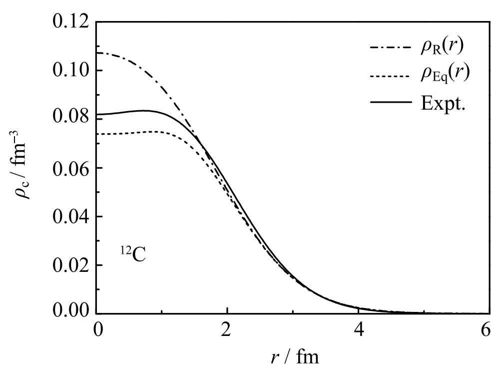

Fig. 2. Charge density distributions of ^{12}C. The dash-dotted line is the RMF charge density $\rho_{\rm R}(r)$ calculated by the FSU parameter set. The solid line is the experimental charge density $\rho_{\rm Ex}(r)$ described by the Fourier-Bessel model, which is taken from Refs. [7, 58]. The dotted line represents the equivalent spherical charge density $\rho_{\rm Eq}(r)$.

In Fig. 1, the charge form factors are calculated under the PWBA method. The initial and final wave functions of electrons in the PWBA method are plane waves, which are not accurate. Therefore, we further investigate the longitudinal form factors by the DWBA method, where the wave functions of scattering electrons are obtained by the exact phase-shift analysis. For nuclei with axial deformation, we use their equivalent spherical charge densities $\rho_{\rm Eq}(r)$ instead of the actual deformed charge densities and solve the Dirac equations of the scattering electrons under the Coulomb potential of $\rho_{\rm Eq}(r)$. The results are presented in Fig.3. Compared with Fig. 1, the DWBA method corrects the discrepancy at the diffraction minima between the theoretical results and experimental data. With the DWBA method, the equivalent spherical charge density $\rho_{\text{Eq}}(r)$ can reproduce the experimental charge form factor well. Results in Fig. 3 show once again that for charge densities expanded with nonorthogonal basis functions, spherical components of all nonorthogonal basis functions can be determined by the C_0 measurements.

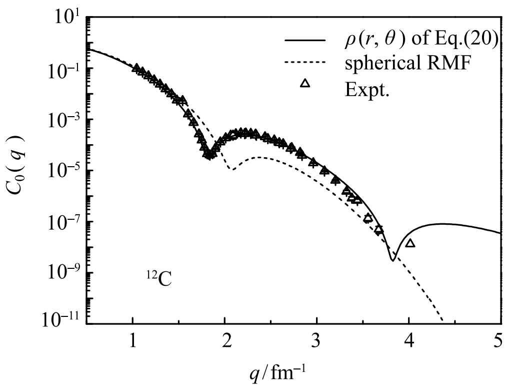

Fig. 3. Same as Fig. 1, but calculated with the DWBA method.

4 Summary

In this paper, the longitudinal form factors of deformed nuclei with rotational symmetry are systematically investigated. By the selection rules, the longitudinal form factors can be decomposed into several multipoles, such as C_0 and C_2. From the intrinsic charge multipoles, C_0 and C_2 of longitudinal form factors are obtained theoretically. The C_2 multipole is closely related to the nuclear quadrupole deformation.

For nuclei with rotational symmetry, the charge density distributions are expanded by both the orthogonal basis functions and nonorthogonal basis functions. With the deformed charge distributions, we derive the C_0 and C_2 multipoles under the PWBA method. It is found that for the charge distribution described by nonorthogonal basis functions, its longitudinal charge form factors are identical with those described by orthogonal basis functions. For even-even nuclei, its longitudinal form factor only contains the C_0 multipole. Therefore, one can use a spherical and phenomenological density (such as a Fermi function) as input to do the DWBA calculations to fit the experimental data.

With the derived formulas, the longitudinal form factors of ^{12}C are calculated by both the PWBA and DWBA methods where the corresponding charge distribution are described by nonorthogonal basis functions. By introducing two tunable parameters into the density profile, the theoretical longitudinal form factors coincide with the experimental data very well. Through the analysis, one can see the equivalent spherical charge distributions extracted from the electron scattering experiments have the same RMS radii as the actual deformed charge distributions. Experiments on electron scattering off exotic nuclei are under way and the results in this paper are useful for the study of structures of exotic nuclei.

References

1 R. Hofstadter, Rev. Mod. Phys., **28**: 214 (1956)
2 Herbert Üerall, *Electron Scattering from Complex Nuclei*, (Academic Press, New York and London, 1971).
3 E. Moya de Guerra, Phys. Rep., **138**: 293 (1986)
4 T. W. Donnelly and I. Sick, Rev. Mod. Phys., **56**, 461 (1984)
5 I. Sick, Prog. Part. Nucl. Phys., **47**: 245 (2001)
6 I. Sick and D. Trautmann, Phys. Rev. C, **89**: 012201 (2014)
7 H. De Vries, C. W. De Jager, and C. De Vries, At. Data Nucl. Data Tables, **36**: 495 (1987)
8 I. Angeli and K. P. Marinova, At. Data Nucl. Data Tables, **99**: 69 (2013)
9 I. Tanihata, Prog. Part. Nucl. Phys., **35**: 505 (1995)
10 A. C. Mueller, Prog. Part. Nucl. Phys., **46**: 359 (2001)
11 T. Suda and M. Wakasugi, Prog. Part. Nucl. Phys., **55**: 417 (2005)
12 H. Simon, Nucl. Phys. A, **787**: 102 (2007)
13 M. Wakasugi et al, Phys. Rev. Lett., **100**: 164801 (2008)
14 T. Suda et al, Phys. Rev. Lett., **102**: 102501 (2009)
15 A. N. Antonov et al, Nucl. Inst. and Meth. in Phys. Res. A, **637**: 60 (2011)
16 A. Antonov et al, Phys. Rev. C, **72**: 044307 (2005)
17 E. D. Cooper and C. J. Horowitz, Phys. Rev. C, **72**: 034602 (2005)
18 X. Roca-Maza, M. Centelles, F. Salvat, and X. Viñas, Phys. Rev. C, **78**: 044332 (2008)
19 Y. Chu, Z. Ren, Z. Wang, and T. Dong, Phys. Rev. C, **82**: 024320 (2010)
20 J. Liu, Z. Ren, C. Xu, and R. Xu, Phys. Rev. C, **88**: 024324 (2013)
21 J. Liu, C. Zhang, Z. Ren, and C. Xu, Chin. Phys. C, **40**: 034101 (2016)
22 X. Roca-Maza, M. Centelles, F. Salvat, and X. Viñas, Phys. Rev. C, **87**: 014304 (2013)
23 K. S. Jassim, A. A. Al-Sammarrae, F. I. Sharrad, and H. A. Kassim, Phys. Rev. C, **89**: 014304 (2014)
24 R. Raphael and M. Rosen, Phys. Rev. C, **1**: 547 (1970)
25 J. Langworthy and H. Überall, Phys. Rev. C, **2**: 911 (1970)
26 B. Downs, D. Ravenhall, and D. Yennie, Phys. Rev., **106**: 1285 (1957)
27 T. Stovall, D. Vinciguerra, and M. Bernherim, Nucl. Phys. A, **91**: 513 (1967)
28 M. K. Pal, Phys. Rev., **117**: 566 (1960)
29 S. S. Avancini, B. V. Carlson, and J. R. Marinelli, Eur. Phys. J. A, **49**: 75 (2013)
30 C. J. Horowitz, Phys. Rev. C, **89**: 045503 (2014)
31 J. M. Yao, M. Bender, and P.-H. Heenen, Phys. Rev. C, **91**: 024301 (2015)
32 R. E. Rand, R. Frosch, and M. R. Yearian, Phys. Rev., **144**: 859 (1966)
33 R. A. Radhi, N. T. Khalaf, and A. A. Najim, Nucl. Phys. A, **724**: 333 (2003)
34 T. Dong, Z. Ren, and Y. Guo, Phys. Rev. C, **76**: 054602 (2007)
35 Z. Wang, Z. Ren, T. Dong, and X. Guo, Phys. Rev. C, **92**: 014309 (2015)
36 D. Yennie, Phys. Rev. C, **95**: 500 (1954)

37 D. H. Jakubassa-Amundsen, J. Phys. G: Nuclear and Particle Physics, **41**: 075103 (2014)
38 E. Moya de Guerra, Phys. Rev. C, **27**: 2987 (1983)
39 M. Nishimura, E. Moya de Guerra, and D. W. L. Sprung, Nucl. Phys. A, **435**: 523 (1985)
40 E. Moya de Guerra, Ann. Phys., **128**: 286 (1980)
41 T. de Forest and J. D. Walecka, Adv. Phys., **15**: 1 (1966)
42 P. Möller, J. R. Nix, W. D. Myers, and W. J. Swiatecki, At. Data Nucl. Data Tables, **59**: 185 (1995)
43 G. Lalazissis and S. Raman, At. Data Nucl. Data Tables, **71**: 1 (1999)
44 S. Raman, C. W. Nestor, and P. Tikkanen, At. Data Nucl. Data Tables, **78**: 1 (2001)
45 N. J. Stone, At. Data Nucl. Data Tables, **90**: 75 (2005)
46 Z. Ren, Z. Y. Zhu, Y. H. Cai, and G. Xu, Phys. Lett. B, **380**: 241 (1996)
47 J. Meng, H. Toki, S. G. Zhou, S. Q. Zhang, W. H. Long, and L. S. Geng, Prog. Part. Nucl. Phys., **57**: 470 (2006)
48 Z. Sheng, Z. Ren, and W. Jiang, Nucl. Phys. A, **832**: 49 (2010)
49 P. Sarriguren, M. K. Gaidarov, E. M. deGuerra, and A. N. Antonov, Phys. Rev. C, **76**: 044322 (2007)
50 E. Moya de Guerra, P. Sarriguren, and J. A. Caballero, Nucl. Phys. A, **529**: 68 (1991)
51 R. S. Willey, Nucl. Phys., **40**: 529 (1963)
52 L. I. Schiff, Phys. Rev., **96**: 765 (1954)
53 Z. Wang and Z. Ren, Phys. Rev. C, **70**: 034303 (2004)
54 B. G. Todd-Rutel and J. Piekarewicz, Phys. Rev. Lett., **95**: 122501 (2005)
55 W.-C. Chen and J. Piekarewicz, Phys. Rev. C, **90**: 044305 (2014)
56 P. E. Hodgson, *Nuclear Reactions and Nuclear Structure* (Clarendon, Oxford, 1971).
57 I. Sick and J. S. McCarthy, Nucl. Phys. A, **150**: 631 (1970)
58 L. S. Cardman, J. W. Lightbody Jr, S. Penner, S. P. Fivozinsky, X. K. Maruyama, W. P. Trower, and S. E. Williamson, Phys. Lett. B, **91**: 203 (1980)